A study of the extreme ultraviolet spectrum of O2 by electron impact

J. M. Ajello and B. Franklin

Citation: The Journal of Chemical Physics **82**, 2519 (1985); doi: 10.1063/1.448301
View online: http://dx.doi.org/10.1063/1.448301
View Table of Contents: http://scitation.aip.org/content/aip/journal/jcp/82/6?ver=pdfcov
Published by the AIP Publishing

A study of the extreme ultraviolet spectrum of O_2 by electron impact

J. M. Ajello and B. Franklin
Jet Propulsion Laboratory, California Institute of Technology, Pasadena, California 91109

(Received 26 March 1984; accepted 28 November 1984)

We have measured in the laboratory the electron impact emission cross sections for O_2 at 200 eV. Included in the study are all emission features in the extreme ultraviolet from 40 to 131 nm at a resolution of 0.5 nm. The features are entirely from the dissociation products (OI, OII, OIII). Additionally we have measured the excitation functions from 0 to 400 eV for characteristic OI multiplets at 98.9 and 102.6 nm and for OII multiplets at 53.9 and 83.3 nm. We find the OI multiplets are formed near the dissociation limit whereas the OII multiplets have a threshold about 10 eV above the dissociation limit. We also determine the total VUV emission cross section of O_2 from 40 to 200 nm and indicate the effects of autoionization to the measured emission spectrum.

INTRODUCTION

Recent studies of O_2 by electron impact have emphasized the importance of dissociative excitation and dissociative ionization excitation processes.[1-3] These dissociative processes are dominant since O_2 does not display molecular emission features in the wavelength range 40–200 nm. In this regard Morgan and Mentall[1] have measured the emission cross sections of about one dozen extreme ultraviolet (EUV) features between 40 and 115 nm at 200 eV. Earlier Zipf *et al.*[2] and McLaughlin[3] of the University of Pittsburgh have measured the emission cross sections and excitation functions for eight features in the wavelength range 80 to 140 nm. We have complemented these earlier studies by measuring the emission cross section at 200 eV for all features (~40 at 0.5 nm resolution) between 40 and 130 nm. Combining these results with earlier work on the 130.4[4-7] and 135.6 nm[5,8] OI multiplets we arrive at the total emission cross section of O_2 for vacuum ultraviolet (VUV) emission between 40 and 200 nm. Many of these OI and OII features have been observed in the Earth's dayglow and aurora, although here the major process is electron excitation of atomic O.[9,10]

EXPERIMENTAL

The experimental apparatus and VUV calibration techniques have been described in detail in earlier publications.[11-13] In brief, the instrument consists of an electron impact emission chamber in tandem with two UV monochromators. A magnetically collimated beam of electrons is crossed with a beam of gas formed by a capillary array at a background pressure that can be varied from 1×10^{-7} to 3×10^{-4} T. The instrument is entirely automated for repetitive scans and interfaced with a computer. The electron gun is mounted on a rotatable table to allow a measurement of the angular distribution of the radiation field in order to correct the measured cross section for polarization effects. However the measurements reported here were made at a 90° angle between electron beam axis and optic axis, since no polarization effects are expected in the case of molecular dissociative excitation where many intermediate states contribute to the dissociation.[14]

The relative sensitivity of the monochromator and channeltron detector as a function of wavelength was determined by two methods which were: (1) double monochromator technique (40–130 nm) and (2) the relative intensities of the H_2 (B, B', B'', C, D, D') band systems (80–130 nm) produced by electron impact. These two methods have been discussed previously.[13] A figure showing the relative sensitivity of the instrument as a function of wavelength was shown in a previous publication.[13] The relative calibration is accurate to 15%.

The absolute cross section of OII (83.3 nm) used to normalize the entire 200 eV EUV spectrum is determined by the relative flow technique developed in our laboratory.[15] In this method the Lyman-α fluorescence signal at 200 eV electron impact energy from H_2, the standard gas, is compared to the fluorescence signal from OII (83.3 nm) emission produced by electron impact at 200 eV on O_2, the unknown gas, at low background pressures in the molecular flow gas regime. The comparisons were made over a range of background gas pressures from 3×10^{-7} to 1×10^{-5} Torr to establish linearity of signal with pressure. For the comparison of the signal strengths in the linear region, a value of 5.78×10^{-18} cm^2 was used for the Lyman-α cross section from H_2 at 200 eV.[16] By this method we find the cross section of the OII (83.3 nm) feature to be 2.15×10^{-18} cm^2 at 200 eV. Other measurements of this cross section are given in Table I. In the relative flow method, where H_2 is used as the standard gas, care must be taken to properly subtract the underlying molecular Lyman and Werner bands from the HI (121.6 nm) signal. We describe this procedure based on our H_2 models[13] in another publication.[16] We judge there is about 15% uncertainty in our published Lyman-α cross section together with a 15% uncertainty in relative

 0021-9606/85/062519-10$02.10

TABLE I. O_2 emission cross sections at 200 eV.

Feature number	Species	Wavelength (nm)	Term	Observed peak wavelength (nm)	Integrated wavelength interval (nm)	Cross section (10^{-19} cm^2)	Other measurements (10^{-19} cm^2)
1	OII	37.6693	$g\,^4S^0$-^4P	...	...	<0.2	
	OII	37.6745	$g\,^4S^0$-^4P				
	OII	37.7045	$g\,^4S^0$-^4D				
	OII	39.1912	$g\,^4S^0$-^4P				
	OII	39.1943	$g\,^4S^0$-^4P				
	OII	39.2002	$g\,^2S^0$-^4P				
	OII	39.2322	$g\,^4S^0$-^4D				
	OII	40.3035	$^2D^0$-^2D				
	OII	40.3087	$^2D^0$-^2D				
	OII	40.3273	$^2D^0$-^2F				
	OII	40.3372	$^2D^0$-^2F				
	OII	41.8598	$g\,^4S^0$-^4P				
	OII	41.8812	$^2D^0$-^2F				
2	OII	42.4577	$^2P^0$-^2S	42.9	42.5–43.5	0.21	
	OII	42.5273	$^2P^0$-^2P				
	OII	42.6526	$^2P^0$-^2D				
	OII	42.9557	$g\,^4S^0$-^2F				
	OII	42.9647	$g\,^4S^0$-^4D				
	OII	42.9716	$g\,^2S^0$-^4D				
	OII	42.9918	$g\,^4S^0$-^4P				
	OII	43.0041	$g\,^4S^0$-^4P				
	OII	43.0177	$g\,^4S^0$-^4P				
3	OII	43.6510	$^2D^0$-^2D	44.3	43.5–45.1	0.32	
	OII	43.6649	$^2D^0$-^2D				
	OII	43.7332	$^2D^0$-^2F				
	OII	43.7683	$^2D^0$-^2F				
	OII	44.0552	$^2D^0$-^2P				
	OII	44.0598	$^2D^0$-^2P				
	OII	44.2001	$^2D^0$-^2D				
	OII	44.2048	$^2D^0$-^2D				
	OII	44.3681	$^2P^0$-^2D				
	OII	44.5601	$^2D^0$-^2F				
	OII	44.5638	$^2D^0$-^2F				
4	OII	45.6997	$^2P^0$-^2D	...	...	<0.2	
	OII	45.8422	$^2P^0$-^2P				
5	OII	46.4194	$^2P^0$-^2D	46.4	46.2–47.1	0.23	
	OII	46.4310	$^2P^0$-^2D				
	OII	46.4785	$^2P^0$-^2S				
	OII	46.5529	$^2P^0$-^2P				
	OII	46.5760	$^2P^0$-^2P				
	OII	46.7926	$^2D^0$-^2P				
	OII	46.8766	$^2P^0$-^2P				
	OII	47.0408	$^2P^0$-^2D				
6	OII	48.1587	$^2D^0$-^2D	48.4	47.8–49.3	1.06	
	OII	48.1635	$^2D^0$-^2D				
	OII	48.1704	$^2D^0$-^2D				
	OII	48.1755	$^2D^0$-^2D				
	OII	48.3752	$^2D^0$-^2P				
	OII	48.3976	$^2D^0$-^2P				
	OII	48.4025	$^2D^0$-^2P				
	OII	48.5086	$^2D^0$-^2F				
	OII	48.5465	$^2D^0$-^2F				
	OII	48.5515	$^2D^0$-^2F				
	OII	48.5572	$^2D^0$-^4D				
	OII	48.5631	$^2D^0$-^4D				
7	OII	49.9871	$^2P^0$-^2P	50.1	49.3–50.8	0.23	
	OII	50.0343	$^2P^0$-^2P				
8	OII	51.5498	$^2P^0$-^2D	51.8	50.8–52.4	0.72	
	OII	51.5640	$^2P^0$-^2D				
	OII	51.7937	$^2P^0$-^2P				
	OII	51.8242	$^2P^0$-^2P				

TABLE I (*continued*).

Feature number	Species	Wavelength (nm)	Term	Observed peak wavelength (nm)	Integrated wavelength interval (nm)	Cross section (10^{-19} cm^2)	Other measurements (10^{-19} cm^2)
9	OII	53.7830	$^2D^0$-^2P	53.9	53.1–54.8	6.89	4.8[a]
	OII	53.8256	$^2D^0$-^2P				
	OII	53.8318	$^2D^0$-^2P				
	OII	53.9086	$g\,^2S^0$-^4P				
	OII	53.9547	$g\,^4S^0$-^4P				
	OII	53.9853	$g\,^4S^0$-^4P				
10	OII	55.5056	$^2D^0$-^2D	55.3	54.8–56.3	2.19	1.1[a]
	OII	55.5121	$^2D^0$-^2D				
11	OII	58.0400	$^2P^0$-^2P	58.0	57.6–58.8	0.29	
	OII	58.0967	$^2P^0$-^2P				
12	OII	60.0585	$^2P^0$-^2D	60.0	59.5–60.9	1.09	
13	OII	61.6291	$^2D^0$-^2P	61.7	60.9–62.6	3.99	1.5[a]
	OII	61.6363	$^2D^0$-^2P				
	OII	61.7051	$^2D^0$-^2P				
14	OII	64.4148	$^2P^0$-^2S	64.3	63.9–65.2	0.61	
15	OII	67.2948	$^2P^0$-^2P	67.3	66.7–68.3	0.73	
	OII	67.3768	$^2P^0$-^2P				
16	OIII	70.2332	$g\,^3P$-$^3P^0$	70.5	70.0–71.3	0.34	
	OIII	70.2822	$g\,^3P$-$^3P^0$				
	OIII	70.2899	$g\,^3P$-$^3P^0$				
	OIII	70.3850	$g\,^3P$-$^3P^0$				
	OIII	70.5762	$^3P^0$-^3P				
	OIII	70.6224	$^3P^0$-^3P				
	OIII	70.6298	$^3P^0$-^3P				
	OIII	70.7315	$^3P^0$-^3P				
17	OII	71.8484	$^2D^0$-^2D	71.9	71.3–72.9	3.88	1.0[a]
	OII	71.8562	$^2D^0$-^2D				
18	OII	73.9949	^4P-$^4S^0$	...	...	<0.2	
	OII	74.0838	^4P-$^4S^0$				
	OII	74.1293	^4P-$^4S^0$				
19	OII	79.6661	$^2P^0$-^2D	79.6	78.9–80.5	0.61	
20	OII	83.2762	$g\,^4S^0$-^4P	83.3	82.9–84.5	21.5	8.8[a]
	OII	83.3332	$g\,^4S^0$-^4P				13.6[b]
	OII	83.4462	$g\,^4S^0$-^4P				13.2[c]
	OIII	83.2927	$g\,^3P$-$^3D^0$				
	OIII	83.3742	$g\,^3P$-$^3D^0$				
	OIII	83.5096	$g\,^3P$-$^3D^0$				
	OIII	83.5292	$g\,^3P$-$^3D^0$				
21	OI	86.163 P	^1D-$^1D^0$	86.0	85.4–86.8	0.48	
22	OI	87.7798	$g\,^3P$-$^3P^0$	87.8	86.8–88.8	4.60	2.5[a]
	OI	87.7879	$g\,^3P$-$^3P^0$				
	OI	87.7201 P	^1D-$^1F^0$				
	OI	87.8972	$g\,^3P$-$^3P^0$				
	OI	87.9019	$g\,^3P$-$^3P^0$				
	OI	87.9100	$g\,^3P$-$^3P^0$				
	OI	87.9551	$g\,^3P$-$^3P^0$				
	OI	88.2890 P	^1D-$^1D^0$				
23	OI	92.2008 P	^1D-$^1F^0$	broad	90.0–93.5	1.44	
	OI	92.2073 P	^1D-$^1D^0$				
	OI	92.9517 P	$g\,^3P$-$^3D^0$				
	OI	93.0257 P	$g\,^3P$-$^3S^0$				
	OI	93.0886 P	$g\,^3P$-$^3D^0$				
	OI	93.1482 P	$g\,^3P$-$^3D^0$				
	OI	93.1628 P	$g\,^3P$-$^3S^0$				
	OI	93.2225 P	$g\,^3P$-$^3S^0$				

TABLE I (*continued*).

Feature number	Species	Wavelength (nm)	Term	Observed peak wavelength (nm)	Integrated wavelength interval (nm)	Cross section (10^{-19} cm^2)	Other measurements (10^{-19} cm^2)
24	OI	93.5193 P	^1D-$^1D^0$	93.6	93.5–94.6	1.22	
	OI	93.6630 P	$g\ ^3P$-$^3D^0$				
	OI	93.7841 P	$g\ ^3P$-$^3S^0$				
	OI	93.8020 P	$g\ ^3P$-$^3D^0$				
	OI	93.8625 P	$g\ ^3P$-$^3D^0$				
	OI	93.9235 P	$g\ ^3P$-$^3S^0$				
	OI	93.9841 P	$g\ ^3P$-$^3S^0$				
25	OI	94.8686	$g\ ^3P$-$^3D^0$	94.9	94.6–95.7	1.20	
	OI	94.0112	$g\ ^3P$-$^3D^0$				
	OI	95.0733	$g\ ^3P$-$^3D^0$				
	OI	95.0885	$g\ ^3P$-$^3S^0$				
	OI	95.2318	$g\ ^3P$-$^3S^0$				
	OI	95.2941	$g\ ^3P$-$^3S^0$				
26	OI	97.1738	$g\ ^3P$-$^3D^0$	97.2	96.6–98.4	3.44	3.41[c]
	OI	97.3234	$g\ ^3P$-$^3D^0$				
	OI	97.3885	$g\ ^3P$-$^3D^0$				
	OI	97.6448	$g\ ^3P$-$^3S^0$				
	OI	97.7959	$g\ ^3P$-$^3S^0$				
	OI	97.8617	$g\ ^3P$-$^3S^0$				
27	OI	98.8578	$g\ ^3P$-$^3D^0$	99.0	98.4–99.8	10.0	9.6[a]
	OI	98.8655	$g\ ^3P$-$^3D^0$				10.1[c]
	OI	98.8773	$g\ ^3P$-$^3D^0$				
	OI	99.0127	$g\ ^3P$-$^3D^0$				
	OI	99.0204	$g\ ^3P$-$^3D^0$				
	OI	99.0801	$g\ ^3P$-$^3D^0$				
28	OI	99.9497	^1D-$^1P^0$	100.0	99.8–100.9	3.18	2.1[a]
29	OI	102.5762	$g\ ^3P$-$^3D^0$	102.7	102.2–103.6	7.08	7.2[a]
	OI	102.7431	$g\ ^3P$-$^3D^0$				8.0[c]
	OI	102.8157	$g\ ^3P$-$^3D^0$				
30	OI	103.9230	$g\ ^3P$-$^3S^0$	104.0	103.6–104.9	2.54	3.3[a]
	OI	104.0943	$g\ ^3P$-$^3S^0$				2.5[c]
	OI	104.1688	$g\ ^3P$-$^3S^0$				
31		Same as feature 9 (second order)					
32		Same as feature 10					
33	OI	115.2151	^1D-$^1D^0$	115.2	114.8–5.9	3.00	4.7[a]
							3.2[c]
34		Same as feature 12					
35	OI	121.7648	^1S-$^1P^0$	121.8	121.6–2.5	1.43	
36		Same as feature 13					
37		Same as feature 14					
38	OI	130.2169 ST	$g\ ^3P$-$^3S^0$	...	...	23.6	23[c]
	OI	130.4858 ST	$g\ ^3P$-$^3S^0$				22[f]
	OI	130.6029 ST	$g\ ^3P$-$^3S^0$				28[d]
							27.6[b]
							19[e]
39	OI	135.5598	$g\ ^3P$-$^5S^0$	...	...		~70[g]
	OI	135.8512	$g\ ^3P$-$^5S^0$				

Important total cross sections at 200 eV

Process	Product	Cross section (10^{-17} cm^2)
Ionization	O_2^+ (200 eV)	26[h]
Dissociative ionization	O^+ (200 eV)	9.9[h]
Dissociative ionization excitation in EUV from allowed states	O^{+*} (200 eV) (allowed states above 4 eV from ground state)	0.45

TABLE I (*continued*).

Important total cross sections at 200 eV

Process	Product	Cross section (10^{-17} cm^2)
Total EUV 38–131 nm	O^*, O^{+*}, O^{++*}	1.08
Total EUV 38–140 nm	O^*, O^{+*}, O^{++*}	1.78
Total EUV 38–140 nm	O_2^*, O_2^{+*} molecular emissions	0.0

[a] H. D. Morgan and J. E. Mentall (Ref. 1) corrected as indicated in the text.
[b] J. F. M. Aarts and F. J. de Heer (Ref. 4).
[c] E. C. Zipf *et al.* (Ref. 2) and R. W. McLaughlin (Ref. 3) corrected as indicated in the text.
[d] J. M. Ajello (Ref. 5).
[e] M. J. Mumma and E. C. Zipf (Ref. 7) corrected as indicated in the text.
[f] G. M. Lawrence (Ref. 6).
[g] W. C. Wells *et al.* (Ref. 8).
[h] D. Rapp *et al.* (Ref. 18) and Kieffer and G. H. Dunn (Ref. 19).

calibration. The signal statistics and repeatability of the measurements provide relative cross sections to 5% accuracy. The resultant root sum square uncertainty is 22% for the absolute cross sections.

It is important to point out at this time that our recent determination[16] of the Lyman-α dissociative excitation cross section from H_2 is 31% below the value determined by Mumma and Zipf.[7] We have revised the Lyman-α cross section based on cross section measurements of the Lyman and Werner bands[16] and our previously measured Lyman-α/Lyman bands and Lyman-α/Werner bands electronic cross section ratios.[13] These results are described in a publication by Shemansky *et al.*[16] The revised value of 5.78×10^{-18} cm^2 at 200 eV reflected in these new measurements was used in the relative flow calibration.

RESULTS

We show in Figs. 1 and 2 the same EUV spectrum for the process $O_2 + e$ (200 eV). In Fig. 1 the spectral features are identified by Rydberg series and/or spectroscopic notation; and in Fig. 2 the features are identified by number. Note the spectrum is only calibrated to 130 nm. Thus features 38 and 39, the 130.4 and 135.6 nm multiplets of OI, are not shown to scale. Additionally we list in Table I the complete set of all OI, OII, and OIII multiplets contributing to each identified feature. These identifications are taken from Kelly and Palumbo.[17] We have determined the cross section for each spectral feature by comparing its area relative to the area of the 83.3 nm spectral feature, whose cross section we have determined by the relative flow technique described above. We also have remeasured the OI (130.4 nm) multiplet with our far ultraviolet (FUV) spectrometer apparatus (110–300 nm).[13]

The last two columns of numbers in Table I compare the cross sections measured in this work to the cross section measurements from previous results.[1–8] Corrections were made to some of the previous works for the new Lyman-α and NI (120.0 nm) calibration standards derived at our laboratory. We have already discussed our new $L\alpha$ result. In the next section we will discuss our new NI (120.0 nm) results as it bears on calibration of previously published electron impact O_2 data. The cross sections given here were obtained by integrating over the wavelength interval in column 5.

At the resolution of the experiment of 0.5 nm there were a total of 39 features observed. Features 1–20 are ionic transitions, mostly OII multiplets; features 21–39 are atomic oxygen multiplets, except for a few second

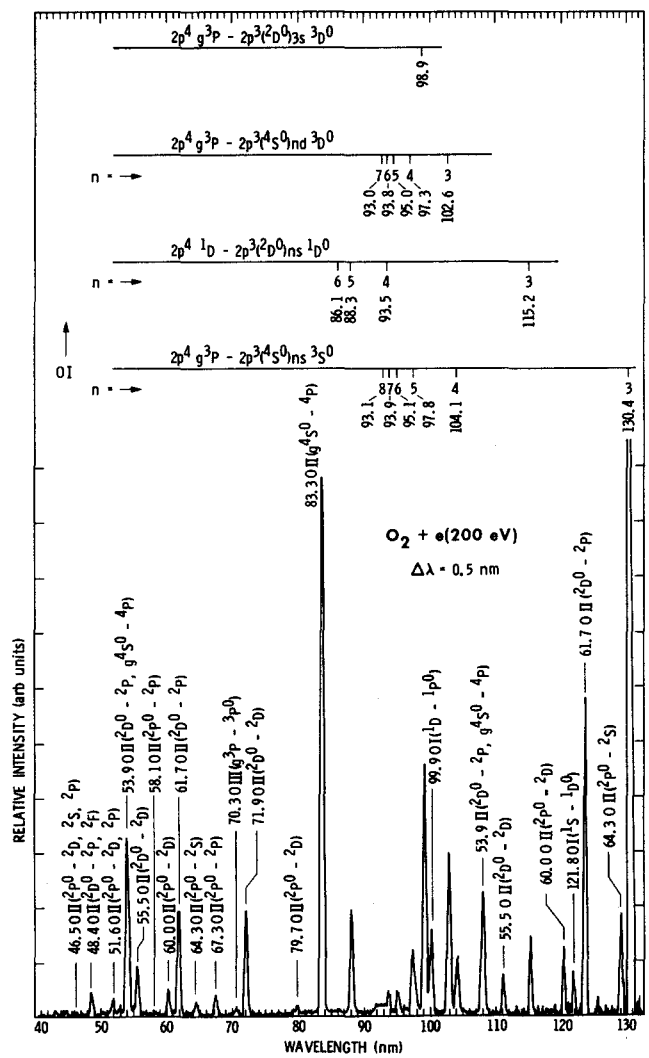

FIG. 1. Calibrated spectrum of O_2 at 200 eV electron impact energy at 0.5 nm resolution from 40 to 130 nm. The spectrum was obtained in the crossed beam mode at 4×10^{-6} Torr background pressure. Many of the features are identified by Rydberg series.

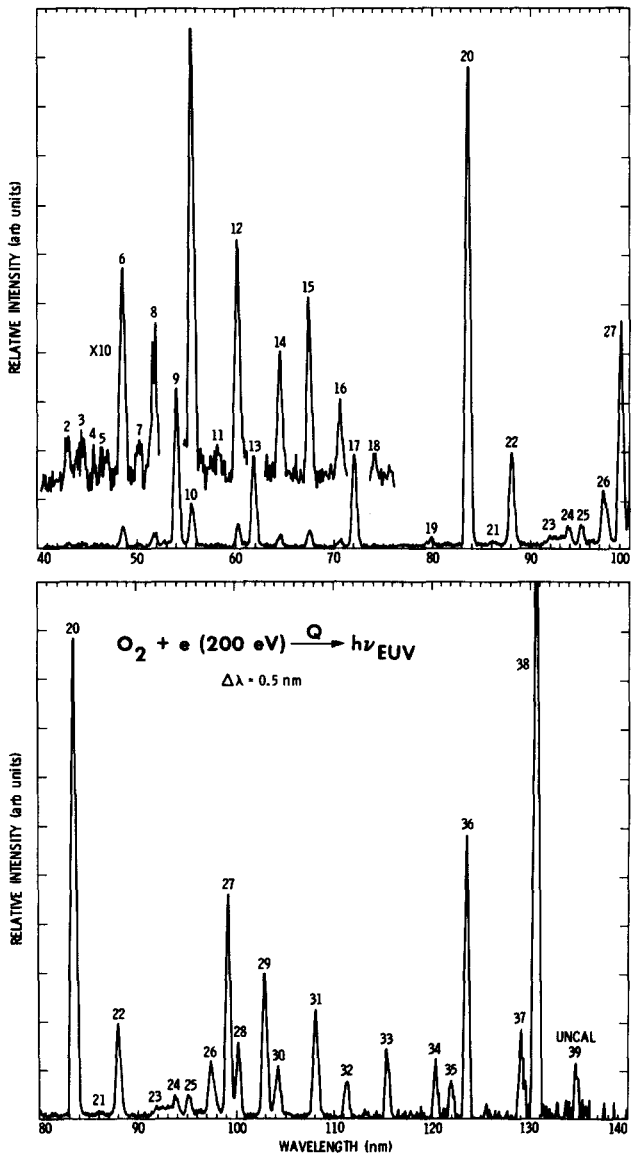

FIG. 2. Calibrated EUV spectrum of O_2 at 200 eV as in Fig. 1. The feature numbers are listed in Table I with identifications and cross sections.

order OII features. Upper limit values are given for (candidate) features 1 and 4. Some features (23, 24, 27, 28) were not completely resolved. The OI features are singlets and triplets (except for the long-lived $^5S^0 \rightarrow g\ ^3P$ transition); the OII features were doublets and quartets; and the single clearly identified feature of OIII was the resonance triplet at 70.5 nm. Note Table I shows that the 83.3 OII feature probably contains a small contribution from the OIII resonance transition at nearly the same wavelength.

At the end of the table we sum the individual contribution from each feature to obtain the total EUV [including the OI (130.4 nm) and OI (135.6 nm) features] cross sections at 200 eV. This cross section is also the total VUV cross section (40–200 nm). We compare these cross sections to other important O_2 cross sections.[18,19] We find, e.g., that the molecular emissions (O_2, O_2^+) yield a zero VUV emission cross section. This result shows the importance of predissociation at energies below the ionization limit at 12.075 eV and of predissociation and autoionization at energies above the ionization limit.

The dissociative ionization process has a total cross section of 9.9×10^{-17} cm^2.[18,19] We measure a VUV emission cross section of 4.5×10^{-18} cm^2 for dissociative ionization excitation. Thus at least 4.5% of the O^+ ions are in excited states, which radiate in the EUV. A list of the near UV-visible-infrared OII features can be found in Wiese *et al.*[20] In future studies we will measure these emissions which represent in many cases a cascade component to the emission cross section results of Table I.

In addition to the electron excited O_2 spectrum at 200 eV we have acquired excitation functions for two OI features and two OII features. These cross section curves are shown in Figs. 3–6 for the OI 102.6 nm, the OI (98.9 nm), the OII (83.3 nm), and the OII (53.9 nm) multiplet features, respectively. The results clearly show that the measured thresholds for the OI multiplets occur close to the dissociation limits whereas the OII multiplets have measured thresholds at nearly 10 eV above the dissociation limit. The dissociation limits and observed thresholds are shown in Table II for one excited and one ground state oxygen atom (ion). The table also includes the dissociation limits for ionization excitation. Possible small breaks in the 98.9 and 102.6 nm near 40 eV are found indicating dissociative ionization is likely. However the sharpness of a break is much less definite than in the corresponding case of N_2 [e.g., NI (120.0, 124.3, 149.3 nm)].[21] In general, for dissociative processes thresholds occur corresponding to dissociation limits of both products in excited states. The peak cross section occurs at ~100 eV for the OI multiplets and 160–200 eV for the OII multiplets.

DISCUSSION

We have presented the emission cross sections for all features excited by electron impact of O_2 in the EUV, 40 to 130 nm. The features are entirely from the dissociation products (OI, OII, OIII). We included in our calculation of the total EUV cross section results from a previous work[8] which have determined an estimate of the 135.6 nm cross section value. There are no molecular emission features from electron impact of O_2 between 40 and 200 nm. Thus this study includes all emissions arising from electron impact of O_2 between 40 and 200 nm and has lead to an estimate of the total VUV cross section of O_2.

The comparisons given in Table I show that our results agree quite well with the previously published data from the University of Pittsburgh. To study this comparison we have corrected the previously published data of Mentall and Morgan[1] (MM) and the University of Pittsburgh[2,3] for the effects of our redetermination of the NI (120.0 nm) cross section. These groups used the NI (120.0 nm) cross section for their absolute calibration. We have measured the NI (120.0 nm) cross section at 100 and 200 eV and find values of 4.48×10^{-18} and 3.48×10^{-18} cm^2, respectively. These results will be described in a future paper. As a calibration standard the revised NI (120.0 nm) cross section has a value at 200 eV that is

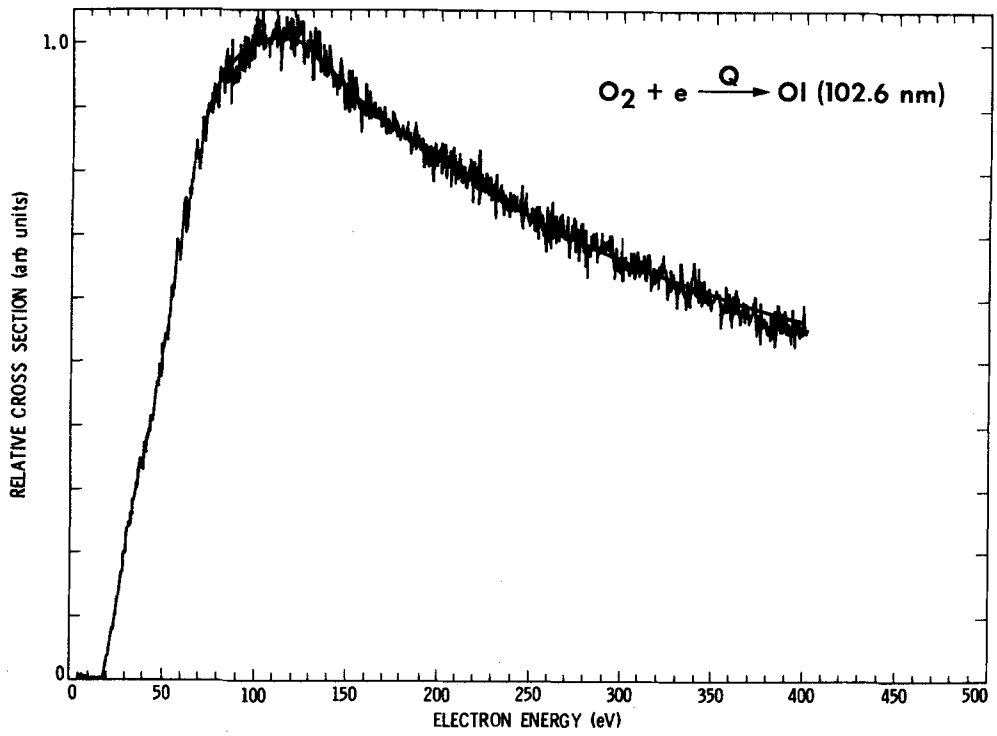

FIG. 3. Relative emission cross section of the OI (102.6 nm) multiplet from 0 to 400 eV.

32% lower than the value of 5.11×10^{-18} cm^2 used by MM and has a value at 100 eV that is 33% lower than the value of 6.7×10^{-18} cm^2 used by the University of Pittsburgh group. Most of this decrease (31%) is due to our revised value for the Lyman-α cross section formerly used as a standard in the NI (120.0 nm) cross section determination. Thus without the revised Lyman-α cross section, the result of Mumma and Zipf for NI (120.0 nm) would be within 2% of the value for the NI (120.0 nm) measured here. Our results in Table I would tend to be significantly higher without the new standard Lyman-α cross section. With this correction applied to the results of MM, the comparison shown in Table I for wavelengths greater than 90 nm indicates that better than 10% agreement is attained for some features (27, 29). On the other hand for wavelengths below 90 nm our results for O_2 tend to be larger than the corrected values of MM. (Refer to feature numbers 9, 10, 13, 17, 20, and 22.) It is significant in a discussion of the OII features that the shape function of the cross section for feature number 20

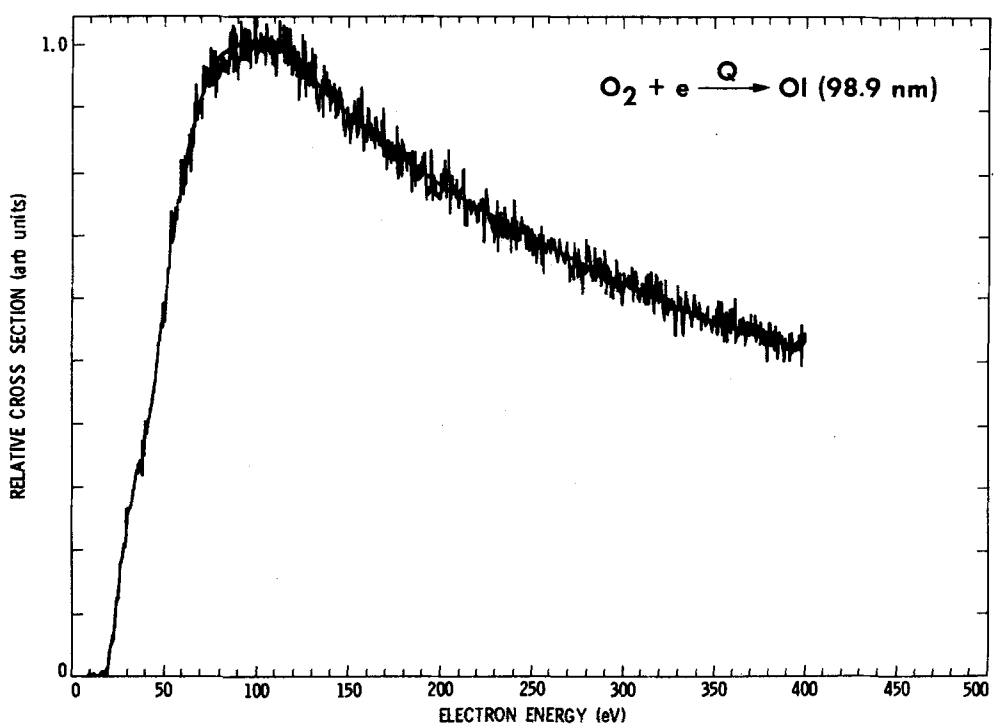

FIG. 4. Relative emission cross section of the OI (98.9 nm) multiplet from 0 to 400 eV.

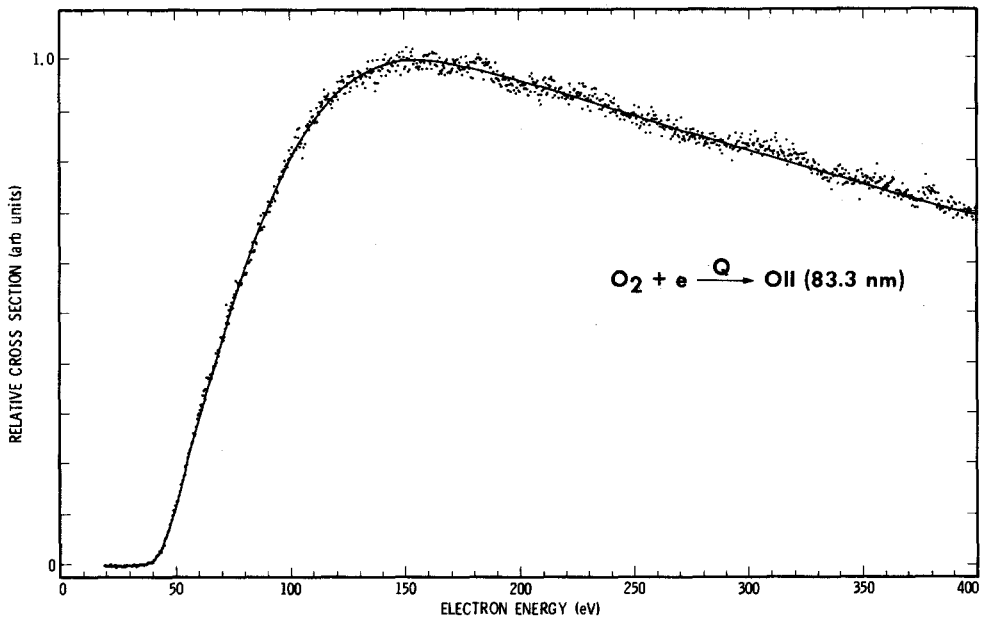

FIG. 5. Relative emission cross section of the OII (83.3 nm) multiplet from 0 to 400 eV.

is different from the results of MM. Compare our Fig. 5 with MM, Fig. 11 for feature number 20, OII (83.3 nm). Perhaps the experiment of MM had a difficulty with electron energy determinations or Faraday cup current measurements. We attribute the remaining experimental differences to both pressure effects and calibration differences. For example, the overall relative intensities of the spectral features at 200 eV [compare our Figs. 1 and 2 with MM, Figs. 9(a) and (b)] are somewhat different even though roughly the same resolutions were present in taking the data. This experiment was conducted at a pressure of 4×10^{-6} Torr whereas the experiments of MM and the University of Pittsburgh were performed at $2\text{–}3 \times 10^{-4}$ Torr gas pressures. With this latter pressure in our system for test purposes; we can induce secondary effects of about a 10% to 25% decrease in the ratio in the intensities of OII multiplets (40–90 nm) to OI multiplets (90–130 nm). This affect which is presently not explained contributes to the fact that some of our cross section values in the 90–130 nm wavelength region tend to be slightly lower than some of the corrected cross section values previously published. For example note feature numbers 29 and 30. Further high pressure studies are required.

From the standpoint of calibration two points need to be made. First, it should be pointed out that our spectrum was obtained with the same relative calibration as used to evaluate our previously published H_2 spectrum.[13] Thus, the spectral intensities from 90 to 130 nm, e.g., are fixed by the calibration from the relative intensities of principally the H_2 Lyman and Werner bands. The relative calibration curves of both MM and our work indicate a lack of high spectral sensitivity in the 120–130 nm wavelength range due to the fall off of channeltron

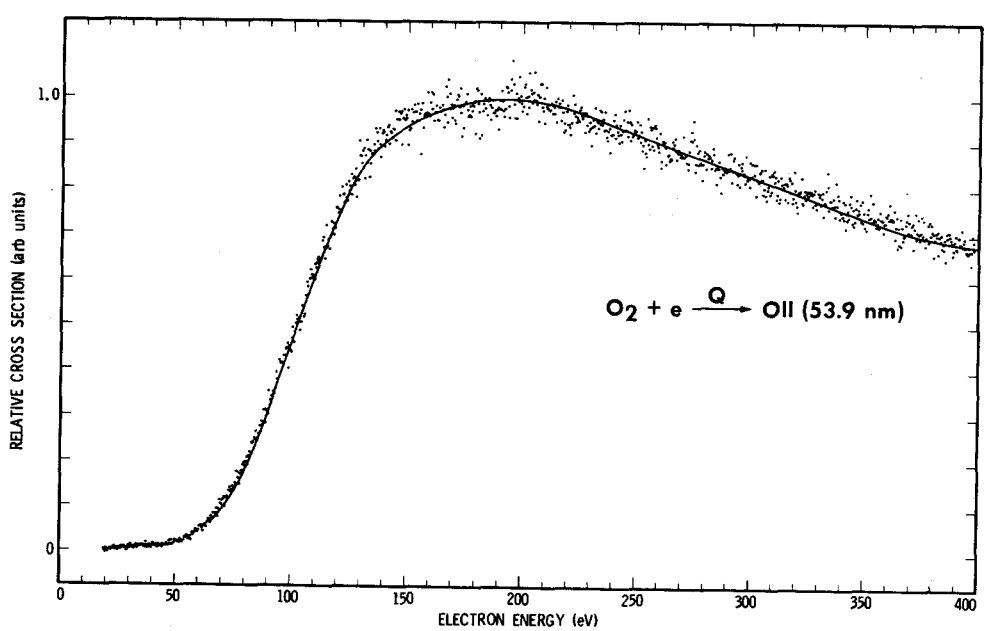

FIG. 6. Relative emission cross section of the OII (53.9 nm) multiplet from 0 to 400 eV.

TABLE II. Dissociative processes for $O_2 + e$.

λ (nm)	Process	Threshold energy: Dissociation limit (eV)	Threshold energy: Observed limit (eV)
102.6	$O_2 + e \rightarrow O(^3D^0) + O(^3P) + e$	17.24	18 ± 1
	$O_2 + e \rightarrow O(^3D^0) + O^+(^4S^0) + e$	30.83	~35–40
98.9	$O_2 + e \rightarrow O(^3D^0) + O(^3P) + e$	17.70	18 ± 1
	$O_2 + e \rightarrow O(^3D^0) + O^+(^4S^0) + e$	31.29	~35–40
83.3	$O_2 + e \rightarrow O^+(^4P) + O(^3P) + e$	33.63	42 ± 3
53.9	$O_2 + e \rightarrow O^+(^4P) + O(^3P) + e$	41.75	52 ± 3
70.9	$O_2 + e \rightarrow O^{++}(^3P) + O(^3P) + e$	71.47	Not measured

response with wavelength. This is an important spectral region since the absolute calibrations were made at NI (120.0 nm) or H_2/HI (121.6 nm) as in the work of MM and this work, respectively. Thus, it appears to be important to verify the accuracy of these calibrations at short wavelengths where the OII cross section measurements are made and where the instrument response is strong. We have satisfactorily checked our short wavelength calibration by remeasuring the HeI (58.4 nm) cross section as discussed earlier. We find, e.g., a direct excitation cross section of He (58.4 nm) at 200 eV of 7.94×10^{-18} cm^2, corrected for polarization and cascading in excellent agreement with Donaldson *et al.*[22] who find a value of 8.18×10^{-18} cm^2. This measurement was made by the relative flow technique in a comparison with Lyman-α emission from H_2. Thus our O_2 cross section results would be the same whether we normalized to HI (121.6 nm) where our optical system had weak sensitivity or to He (58.4 nm) where our optical system has high sensitivity.

Autoionization appears to have a very important effect on the spectrum. First it tends to weaken or totally eliminate certain Rydberg series members. Second it eliminates cascading in all Rydberg series except for the $2p^3(^4S^0)\ ns(^3S^0, {}^5S^0)$ series, the first members ($n = 3$) are the upper states of the 130.4 and 135.6 nm multiplets, respectively. All other $n = 3$ series (e.g., upper states of 121.8, 115.2, 98.9, 87.8 nm transitions) have less than 5% cascade contribution.[6] The $^4S^0$ continuum begins at 13.618 eV and the ^2D continuum at 16.942 eV. The OI multiplet with the highest excitation energy that is observed is the OI (86.1 nm) multiplet $2p^3(^2D^0)\ 6s(^1D^0) \rightarrow 2p^4(^1D)$ with excitation energy 16.35 eV. Rydberg series requiring higher excitation are absent due to autoionization and include the $2p^3(^2D^0)\ nd(^3P^0)\ n \geq 3 \rightarrow 2p^4(g^3P)$ series (see Kelly and Palumbo[17]). There are very few singlet transitions clearly identified. They include the OI (121.8 nm), OI (115.2 nm), OI (99.9 nm), OI (86.1 nm). There are undoubtedly other singlet transitions occurring but higher resolution is needed to resolve them. The OI (115.2 nm) transition is the only singlet transition unaffected by autoionization. The upper $^1D^0$ state is at 12.37 eV. Thus the triplet systems dominate the emission spectrum, particularly the strong $2p^3(^4S^0)\ ns(^3S^0)$ system identified in Fig. 1 whose limit is the $^4S^0$ ionization continuum. It is to be expected that autoionization has similar effects on the spectral intensities resulting from e + O electron impact excitation.

The relative intensities of the OI (99.9 nm) and OI (121.8 nm) transitions, feature numbers 28 and 35, respectively, in Table I, are connected by branching ratio considerations since they originate from the same $3s\ ^1P^0$ upper term. Pradhan and Saraph[23] determine theoretically this branching ratio to be A(99.9 nm)/A(121.8 nm) = 2.58 ± 0.26. Similarly Wiese, Smith, and Glennon[20] determine theoretically that A(99.9 nm)/A(121.8 nm) = 1.95 ± 1.4. We find an experimental value of 2.22 ± 0.55 in good agreement with theoretical calculations. Our uncertainty is slightly larger than the root sum square uncertainty of each of the relative cross sections, since the 99.9 nm feature is not completely resolved in Figs. 1 and 2.

Previous studies of the near threshold behavior of the emissions from the process of dissociative excitation have been conducted by both electron[1–3] and photon[24,25] impact experiments. The observed thresholds in these studies are in agreement and indicate that the radiation is present at the spectroscopic threshold. For example, Carlson[24] has found that in photodissociation of O_2 the OI (130.4 nm) multiplet is detected close to the dissociation limit of 14.59 eV. The Carlson work shows that one possible combination of states for the two dissociated atoms involves the $^3S^0$ excited state and the ^3P ground state. His results also show that the OI (130.4 nm) multiplet is formed by both predissociation and direct dissociation. Predissociation in this case is the process which leads to the observation of the excited atom near the dissociation limit by a predissociating state of $^3\Pi_u$ configuration. Presumably most of the OI features observed in this experiment, having theoretical dissociation limits of 14–20 eV can be produced by either direct excitation and/or predissociation.

On the other hand electron impact experiments on O_2 indicate that the OII features are predominantly formed with a kinetic energy near 10 eV. Freund[26] has detected high Rydberg oxygen atoms from electron impact of O_2 in a time of flight apparatus. One of the processes he detected has an observed threshold in the 37–44 eV region. The observed threshold value is close to that measured in electron impact emission experiments for the dissociative ionization process leading to the 83.3 nm emission. The emission experiments have found that the observed threshold is offset from the dissociation limit as follows: 4–6 eV, Sroka[27] and 10 eV, this work and MM.[1] Freund suggests ionization occurs by removal of a $\sigma_g 2s$

electron into a stable, excited state which is predissociated by a repulsive state from the $O(^3P) + O^+(^4P)$ limit with a subsequent release of kinetic energy. An equally likely possibility is direct dissociative ionization from a potential energy curve which represents a purely repulsive state. Presumably most of the OII emission multiplets have threshold energies that differ by 4–13 eV from their dissociation limits. We find, e.g., a similar result in Table II for the OII 53.9 multiplet. The gradual onset of the OII (53.9 nm) emission is to be expected since two different multiplets underlie the measured feature. Each multiplet has its own set of slightly different threshold energies. In fact many of the features identified in this study are a blend of two or more multiplets. It is recommended that a high resolution study be performed for the EUV spectral region in order to resolve these multiplets.

ACKNOWLEDGMENTS

This work was supported by the Air Force Office of Scientific Research (AFOSR), Planetary Atmospheres and Astronomy/Relativity Programs of NASA. It represents one phase of work sponsored by NASA under Contract NAS7-100 to the Jet Propulsion Laboratory, California Institute of Technology, Pasadena, CA 91109.

[1] H. D. Morgan and J. E. Mentall, J. Chem. Phys. **78,** 1747 (1983).
[2] E. C. Zipf, R. W. McLaughlin, and M. R. Gorman, Planet. Space Sci. **27,** 719 (1979).
[3] R. W. McLaughlin, Ph.D. thesis, University of Pittsburgh, 1977.
[4] J. F. M. Aarts and F. J. de Heer, Physica **56,** 294 (1971).
[5] J. M. Ajello, J. Chem. Phys. **55,** 3156 (1971).
[6] G. M. Lawrence, Phys. Rev. A **2,** 397 (1970).
[7] M. J. Mumma and E. C. Zipf, J. Chem. Phys. **55,** 1661 (1971).
[8] W. C. Wells, W. L. Borst, and E. C. Zipf, Chem. Phys. Lett. **12,** 288 (1971).
[9] E. P. Gentieu, P. D. Feldman, and R. R. Meier, Geophys. Res. Lett. **6,** 325 (1979).
[10] H. Park, P. D. Feldman, and W. G. Fastie, Geophys. Res. Lett. **4,** 41 (1977).
[11] J. M. Ajello and S. K. Srivastava, J. Chem. Phys. **75,** 4454 (1981).
[12] J. M. Ajello, S. K. Srivastava, and Y. L. Yung, Phys. Rev. A **25,** 2485 (1982).
[13] J. M. Ajello, D. Shemansky, T. L. Kwok, and Y. L. Yung, Phys. Rev. A **29,** 636 (1984).
[14] R. J. Van Brunt and R. N. Zare, J. Chem. Phys. **48,** 4304 (1968).
[15] S. K. Srivastava, A. Chutjian, and S. Trajmar, J. Chem. Phys. **63,** 2659 (1975); S. Trajmar and D. Register, *Electron Molecule Collisions,* edited by K. Takayanagi and I. Shimamura (Plenum, New York, 1984), Chap. 6.
[16] D. E. Shemansky, J. M. Ajello, and D. T. Hall, Astrophys. J. (in press).
[17] R. L. Kelly and L. J. Palumbo, NRL Report 7599, pp. 46–52 (1973).
[18] D. Rapp, D. Englander-Golden, and D. D. Briglia, J. Chem. Phys. **42,** 4081 (1965).
[19] L. J. Kieffer and G. H. Dunn, Rev. Mod. Phys. **38,** 1 (1966).
[20] W. L. Wiese, M. W. Smith, and B. M. Glennon, *Atomic Transition Probabilities. Vol. 1. Hydrogen Through Neon,* Natl. Stand. Ref. Data Ser. 1 NSRDS-NBS4 (U.S. GPO, Washington, D.C., 1966).
[21] M. J. Mumma and E. C. Zipf, J. Chem. Phys. **55,** 5582 (1971); J. M. Ajello, *ibid.* **53,** 1156 (1970).
[22] F. G. Donaldson, M. A. Hender, and J. W. McConkey, J. Phys. B **5,** 1192 (1972).
[23] A. K. Pradhan and H. E. Saraph, J. Phys. B **10,** 3365 (1977).
[24] R. W. Carlson, Ph.D. thesis, University of Southern California, 1970.
[25] L. C. Lee, R. W. Carlson, D. L. Judge, and M. Ogawa, J. Chem. Phys. **61,** 3261 (1974).
[26] R. S. Freund, J. Chem. Phys. **54,** 3125 (1971).
[27] W. Sroka, Z. Naturforsch. Teil A **23,** 2004 (1968).